MITSUBISHI ELECTRIC RESEARCH LABORATORIES
http://www.merl.com

# Non-Coherent TOA Estimation in IR-UWB Systems with Different Signal Waveforms

I. Guvenc, Z. Sahinoglu, A. Molisch, P. Orlik

TR2005-132 December 2005

**Abstract**

In this paper, signal waveform designs for TOA estimation with non-coherent receivers based on ultrawideband impulse radio are discussed. Four different transmit signal waveforms are analyzed, both with respect to their design constraints, and their precision ranging performance in IEEE 802.15.4a multipath channels. We introduce novel searchback and thresholding algorithms, and show that the ranging performance can be improved considerably with a-priori knowledge of noise variance. Simulation results show that it is possible to achieve sub-meter ranging accuracy with 90% confidence by using such energy detecting (non-coherent) receivers.

*IEEE BroadNets, October 2005*

# Non-coherent TOA Estimation in IR-UWB Systems with Different Signal Waveforms

I. Guvenc[1,2], Z. Sahinoglu[1], A. F. Molisch[1,3], P. Orlik[1]
[1]Mitsubishi Electric Research Labs, 201 Broadway Ave., Cambridge, MA, 02139
[2]Department of Electrical Engineering, University of South Florida, Tampa, FL, 33620
[3] also at Department of Electronscience, Lund University, Lund, Sweden
E-mail:{guvenc, zafer, molisch, porlik}@merl.com

***Abstract*— In this paper, signal waveform designs for TOA estimation with non-coherent receivers based on ultrawideband impulse radio are discussed. Four different transmit signal waveforms are analyzed, both with respect to their design constraints, and their precision ranging performance in IEEE 802.15.4a multipath channels.**

**We introduce novel searchback and thresholding algorithms, and show that the ranging performance can be improved considerably with a-priori knowledge of noise variance. Simulation results show that it is possible to achieve sub-meter ranging accuracy with 90% confidence by using such energy detecting (non-coherent) receivers.**

## I. Introduction

There is a growing demand for location awareness and ranging in short-range communication networks, and applications exploiting these features will play an important role in future wireless markets. Especially, a variety of control and monitoring applications (e.g., building automation, environmental and structural monitoring etc.) is to be built, using a vast number of short-range, networked wireless devices.

Recognizing these trends, the IEEE has established the IEEE 802.15.4a Task Group (TG), whose goal it is to to develop a low complexity, low rate physical (PHY) layer standard with a precision ranging capability, and it has adopted ultrawideband (UWB) as the underlying technology. Low complexity, and thus low cost, of the devices is an important goal of the standard, and therefore it is required to enable UWB-based ranging with noncoherent (energy detection) receivers. Though their performance (precision or reliability) will be less than that of coherent devices, the reduced cost justifies the tradeoff for many applications. In this paper, we quantify the ranging performance of non-coherent UWB impulse radio (IR) receivers.

A UWB signal provides two major advantages for ranging applications. If the signal has a large relative bandwidth, there is a higher probability that at least some of the frequency components of the transmit signal can penetrate through obstacles. Thus, the probability of receiving significant energy in the quasi-line-of-sight component is larger in this case. Secondly, a large absolute bandwidth implies a fine time resolution of the received signal, which helps to identify the time-of-arrival (TOA) of the multipath components, and improves leading signal edge detection performance. Ranging based on the TOA of the first arriving multipath component (quasi-line-of-sight) is the method of choice for UWB-based ranging [1].

To our knowledge, there are only a few papers in the literature where the ranging performance of non-coherent or differential UWB receivers is studied. In [2], the detection performance of autocorrelation receivers (transmitted reference (TR) and differential (DF) schemes) is studied with respect to different synchronization accuracy levels. Another work [3] presents synchronization analysis of non-coherent UWB receivers for both additive white Gaussian noise (AWGN) and Saleh-Valenzuela channel models, and points out the suitability of non-coherent receivers to enable low cost wireless sensor devices. Low probability of intercept performance of a time-hopping UWB system is investigated in [4] by using a single and multiple energy detectors.

A key problem, which to our knowledge has not been studied in the past, is that precision ranging not only relies on acquisition and coarse synchronization, but also requires additional signal processing and air time to detect the first arriving multipath component (MPC). In typical non line of sight channels this component may be 6dB less than the strongest component, and it may even arrive up to 60ns earlier [5]. In this article, we introduce a leading edge searching and thresholding algorithm designed to deal with this problem, and test its ranging performances on four different ranging transmit signal waveform, which are under consideration by the IEEE 802.15.4a TG. The key contribution of our work is the introduction of a threshold mechanism that is based on the noise level and the clustering of the received multipath components.

## II. Signaling Waveforms

The waveform of the transmitted signal has a significant impact on the performance of the TOA estimation algorithms. By changing placement and number of UWB pulses in a symbol and their relative distance in time and by varying symbol duration, unique symbol waveforms can be generated for use in ranging preambles. These parameters impact the level of inter-pulse-interference and inter-symbol interference, and necessitate development of post reception signal processing algorithms to achieve precision ranging with each specific waveform. In this section, four different signaling waveforms are presented, and their characteristics and trade-off's are discussed. While designing the waveforms, the following design issues and constraints are considered

- The maximum excess delay (MED) of the channel may be on the order of 100ns or larger. The signaling waveform should have a large enough zero correlation zone prior to the leading edge to minimize self-interference.
- If multiple pulses per symbol are transmitted, and the duration between pulses is smaller than the MED of the

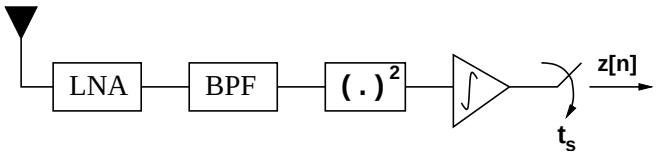


Fig. 1. Sampling the received waveforms.

channel, aggregating the energies over multiple pulses may smooth the edges (due to interpulse interference), and it may be better to operate on the non-aggregated samples for edge detection (e.g. for direct-sequence (DS)-IR).

- Peak to average power ratio (PAPR) and spectral mask requirements of frequency regulators (in particular, the USA's FCC) should be obeyed. Namely, the pulse-to-pulse interval cannot be larger than a certain value, and the spectral peaks should be suppressed via appropriate methods.
- Ranging accuracy should be on the order of 1 meter or better; this value stems from the IEEE 802.15.4a list of requirements.
- While non-coherent receiver processing will be considered in this paper, it is beneficial that the received waveforms also support coherent processing, since this allows dual-mode operation and/or multiple receiver types.

Under these design constraints, signaling waveforms for DS-IR, TR-IR, M-ary ternary orthogonal keying (MTOK)-IR, and time hopping (TH)-IR will be presented below. The common notations for all signaling schemes are as follows; $N_{sym}$ is the number of symbols over which the received samples are averaged, $E_s$ is the symbol energy, $\omega$ is the transmitted pulse shape with unit energy, $T_{sym}$ is the symbol duration, $T_p$ is the pulse duration, $\epsilon$ is the TOA of the waveform, $\eta$ is the zero-mean AWGN with variance $\sigma_n^2 = \frac{N_0}{2}$, $L$ is the total number of multipath components, $\gamma_l$ and $\tau_l$ are the amplitudes and delays of the $l$th multipath component, and $N_s$ is the total number of pulses per symbol. Due to the waveform parameters assumed in this paper (as will be discussed later in the simulation section and illustrated in Table I and Fig. 2), the parameters $E_s$, $N_s$, $N_{sym}$, and $T_{sym}$ are identical for DS-IR, TR-IR, and TH-IR. They are scaled appropriately for MTOK-IR to make transmitted energy per pulse and number of pulses transmitted within unit time identical and fair for all the four options.

### A. DS-IR

The DS-IR waveform is obtained by consecutive transmission of pulses with different polarities, and the received DS-IR waveform can be represented as

$$r^{(ds)}(t) = \sqrt{\frac{E_s}{N_s}} \sum_{k=1}^{N_{sym}} \omega_{mp}^{(ds)}\big(t - kT_{sym} - b_k T_{ppm} - \epsilon\big) + \eta(t) \ , \tag{1}$$

$$\omega_{mp}^{(ds)}(t) = \sum_{l=1}^{L} \gamma_l \sum_{j=1}^{N_s} d_j^{(ds)} \omega\Big(t - (j-1)T_c^{(ds)} - \tau_l\Big) \ , \tag{2}$$

where $d_j^{(ds)}$ is the polarity code for the $j$th pulse, $b_k \in \{0, 1\}$ is the $k$th symbol, $T_{ppm}$ is the modulation index (i.e. delay) for pulse position modulation (PPM), and $T_c^{(ds)} \geq T_p$ is the chip duration for DS-IR. Note that PPM is used to achieve piconet isolation, where different users employ different symbol sequences (which resembles a 2-level *bulk* time hopping).

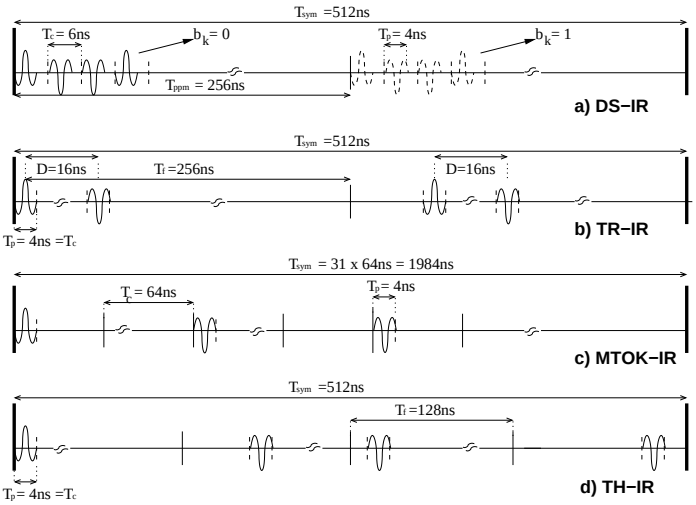


Fig. 2. Signaling waveform options for TOA estimation.

At the receiver, the energy detector output is given by

$$z_n^{(ds)} = \frac{1}{N_{sym}} \sum_{k=1}^{N_{sym}+1} \int_{(n-1)t_s}^{nt_s} \Big| r(t - kT_{sym} - b_k T_{ppm}) \Big|^2 dt \ , \tag{3}$$

where the multiple pulses within the symbol are not aggregated, since they are very closely spaced and thus suffer from interpulse interference; aggregating them thus would smoothen and weaken the edges.

### B. TR-IR

The TR-IR transmits a pair of pulses within each frame, and the received signal can be formulated as

$$r^{(tr)}(t) = \sqrt{\frac{E_s}{N_s}} \sum_{k=1}^{N_{sym}} \omega_{mp}^{(tr)}\big(t - kT_{sym} - \epsilon\big) + \eta(t) \ , \tag{4}$$

$$\omega_{mp}^{(tr)}(t) = \sum_{l=1}^{L} \gamma_l \sum_{j=1}^{N_s/2} \Big[ d_j^{(r)} \omega\Big(t - (j-1)T_f^{(tr)} - c_j^{(tr)} T_c^{(tr)} - \tau_l\Big) + d_j^{(d)} \omega\Big(t - (j-1)T_f^{(tr)} - c_j^{(tr)} T_c^{(tr)} - \tau_l - D\Big)\Big] \ , \tag{5}$$

where $D$ is the delay between the pulse pairs, $c_j^{(tr)}$ denotes the time hopping code (specific to the piconet), $d_j^{(r)}$ and $d_j^{(d)}$ denote the polarity codes of the reference and data pulses in TR, respectively, $T_f^{(tr)}$ is the frame duration, and $T_c^{(tr)}$ is the chip duration.

Since the time duration between the pulse pair is usually smaller than the MED of the channel $\big(\text{i.e., } D < \max(\tau_l)\big)$, aggregating the energy in the pulse pair usually smoothes the

edges, and is not preferred. Therefore, the receiver processing may be achieved as follows

$$z_n^{(tr)} = \frac{1}{N_{sym}} \sum_{k=1}^{N_{sym}+1} \sum_{j=1}^{N_s/2} \int_{(n-1)t_s}^{nt_s} \Big| r\Big(t - kT_{sym} - (j-1)T_f^{(tr)} - c_j^{(tr)} T_c^{(tr)}\Big)\Big|^2 dt \ . \quad (6)$$

### C. MTOK-IR

Instead of binary sequences used in DS-IR, ternary sequences [6] can be used to generate a MTOK-IR signal, and the received signal becomes

$$r^{(mt)}(t) = \sqrt{\frac{E_s^{(mt)}}{N_s^{(mt)}}} \sum_{k=1}^{N_{sym}^{(mt)}} \omega_{mp}^{(mt)}\big(t - kT_{sym}^{(mt)} - \epsilon\big) + \eta(t) \ , \quad (7)$$

$$\omega_{mp}^{(mt)}(t) = \sum_{l=1}^{L} \gamma_l \sum_{j=1}^{N_c^{(mt)}} d_j^{(mt)} \omega\Big(t - (j-1)T_c^{(mt)} - \tau_l\Big) \ , \quad (8)$$

where $d_j^{(mt)} \in \{-1, 0, 1\}$ are the ternary codes for the $j$th pulse. The codeword length is $N_c^{(mt)}$, and the number of non-zero codeword elements (i.e., the number of pulses) is denoted by $N_s^{(mt)}$. The symbol energy, number of symbols used, and the symbol duration are given by $E_s^{(mt)}$, $N_{sym}^{(mt)}$, and $T_{sym}^{(mt)}$, respectively.

The samples collected at the receiver are processed as follows

$$z_n^{(mt)} = \frac{1}{N_{sym}^{(mt)}} \sum_{k=1}^{N_{sym}^{(mt)}+1} \sum_{j=1}^{N_c^{(mt)}} \int_{(n-1)t_s}^{nt_s} \Big| r\Big(t - kT_{sym}^{(mt)} - (j-1)T_c^{(mt)}\Big)\Big|^2 d_j^{(tmplt)} dt \quad (9)$$

where $d_j^{(tmplt)}$ is the template correlation sequence used at the receiver, and is given by

$$d_j^{(tmplt)} = \begin{cases} |d_j^{(mt)}| & \text{if uni-polar template (UPT),} \\ 2 \times |d_j^{(mt)}| - 1 & \text{if bi-polar template (BPT),} \end{cases} \quad (10)$$

where the MTOK sequences can be appropriately designed to have zero autocorrelation sidelobes after they are processed with the BPT at the receiver (which is assumed in the sequel).

### D. TH-IR

As the last signaling waveform, the received TH-IR signal can be expressed as

$$r^{(th)}(t) = \sqrt{\frac{E_s}{N_s}} \sum_{k=1}^{N_{sym}} \omega_{mp}^{(th)}\big(t - kT_{sym} - \epsilon\big) + \eta(t) \ , \quad (11)$$

$$\omega_{mp}^{(th)}(t) = \sum_{l=1}^{L} \gamma_l \sum_{j=1}^{N_s} d_j^{(th)} \omega\Big(t - (j-1)T_f^{th} - c_j^{(th)} T_c^{(th)} - \tau\Big) \quad (12)$$

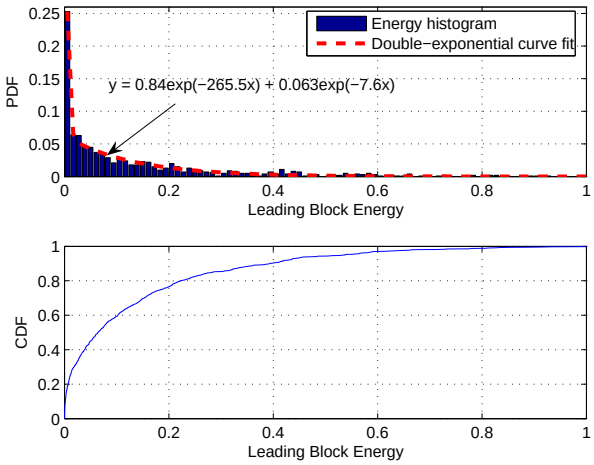


Fig. 3. PDF and CDF of the energy in the leading energy block, and corresponding quadratic curve-fit for the energy PDF (1000 CM1 realizations [5]). The transmitted energy is set to unity ($T_p = t_s = 4$ns), a single pulse is transmited, and sampled with an energy detector at the receiver.

where $c_j^{(th)}$ and $d_j^{(th)}$ are the TH codes and polarity scrambling codes of desired user, respectively. Frame and chip duration of of TH-IR are denoted by $T_f^{(th)} = 0.5T_f^{(tr)}$, and $T_c^{(th)} = T_c^{(tr)}$, respectively.

At the receiver, the samples are collected and processed as follows for the TH-IR signal

$$z_n^{(th)} = \frac{1}{N_{sym}} \sum_{k=1}^{N_{sym}+1} \sum_{j=1}^{N_s} \int_{(n-1)t_s}^{nt_s} \Big| r\Big(t - kT_{sym} - (j-1)T_f^{(th)} - c_j^{(th)} T_c^{(th)}\Big)\Big|^2 dt \ . \quad (13)$$

## III. Threshold Selection for TOA Estimation

The TOA estimation algorithm is closely tied to the acquisition scheme employed in the transceiver. In this paper, we assume that the transmitted signal contains a preamble that is long enough to allow accurately synchronize the receiver to the peak energy sample and subsequently estimate the TOA. Since the TOA estimation requires estimation of the leading edge, the samples prior to the peak have to be searched and distinguished from the noise level. However, the leading block's energy may be very small compared to the total transmitted energy, since the energy is distributed over various multipath components. In Fig. 3, about 10% of the time, the leading block energy is seen to be considerably small compared to the transmitted energy for CM1, which emphasizes the importance of threshold selection.

In [7], threshold selection was achieved by simply setting the thresholds based on a normalized value between the minimum and maximum energy samples. Even though this technique accounts both the signal and noise energy levels, and does not require any parameter estimation, relatively weak leading edge samples (compared to the peak) can be missed. In Fig. 4a, the cumulative distribution function (CDF) of the maximum energy to leading edge energy ratio (MER) is given for 1000 CM1 channel realizations. Since it may occur that only a small portion of the leading pulse energy is contained

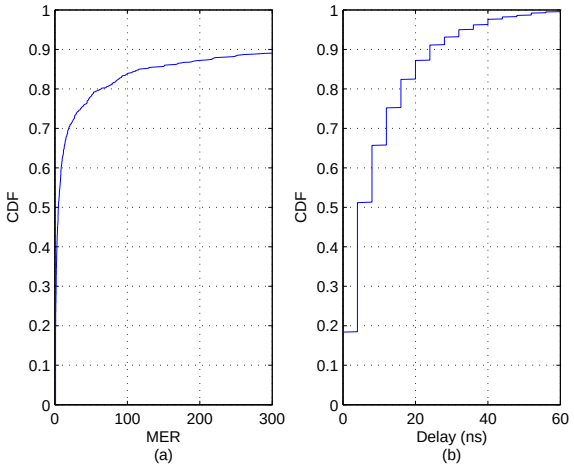


Fig. 4. a) The CDF of MER, b) The delay between the energy peak and the leading edge for CM1 ($T_p = t_s = 4$ns).

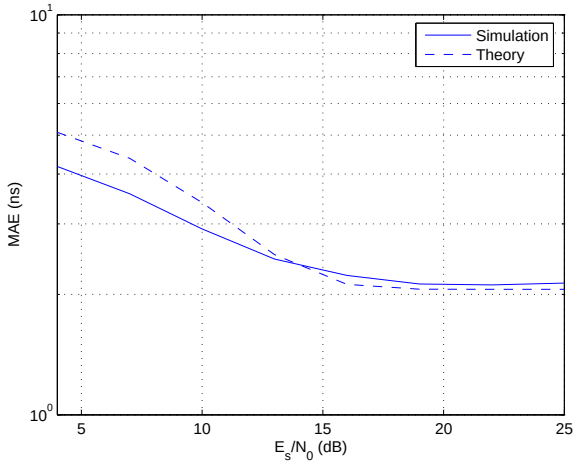


Fig. 5. Theoretical and simulation MAE of the TOA estimates for a 2-tap channel ($P_{fa} = 0.05$).

in the leading energy block, the MER can be as large as 40dB (not shown on plot), and is smaller than 300 with 90% probability. Therefore, setting the normalized threshold to $1/300$ will miss 10% of the leading edge blocks in noise-free channel. On the other hand, Fig. 4b shows that the delay between the peak and the leading edge may be as large as 60ns for CM1, which we set our searchback window length.

Another alternative for setting the thresholds is using solely the noise level, which has to be estimated prior to leading edge detection. Let $\mu_{ed}$ and $\sigma_{ed}^2$ be the mean and the variance of the noise samples that are at the output of the energy detector, and after any processing gain (multiple pulses per symbol, or multiple symbols). Then, the probability of erroneously interpreting a noise sample as a signal sample is

$$P_{fa} = Q\left(\frac{\xi - \mu_{ed}}{\sigma_{ed}}\right) , \qquad (14)$$

where $\xi$ denotes a threshold, $\mu_{ed} = M\sigma_n^2$, $\sigma_{ed}^2 = 2M\sigma_n^4$, and $M = 2Bt_s$ is the degree of freedom determined by the signal bandwidth (determined by the band-pass filter) and the sampling rate. Note that (14) assumes a Gaussian approximation to the Chi-square statistics, which is valid for large $M$, or large processing gain, and is valid for large $N_{sym}$ assumed in this paper. By fixing $P_{fa}$, $\xi$ can be calculated from (14) as

$$\xi = \sigma_{ed} Q^{-1}(P_{fa}) + \mu_{ed} . \qquad (15)$$

If there are no *noise-only* samples between the leading edge and the peak, the thresholding technique discussed above successfully tracks the samples till the leading edge, and the leading block estimate is given by

$$\hat{n} = \text{First}\left\{ n' \,\middle|\, \tilde{z}_{n'} > \xi \text{ and } \tilde{z}_{n'-1} < \xi \right\} + n_{mx} - w_{sb} , \qquad (16)$$

where the hypothesis $n' \in \{1, 2, ..., w_{sb} - 1, w_{sb}\}$ are tested backwards starting from $n' = w_{sb}$ down to $n' = 1$, $n_{mx}$ is the sample index for the peak energy, the search-back vector is given by

$$\tilde{z} = \left[ z_{n_{mx} - w_{sb}} \quad z_{n_{mx} - w_{sb}+1} \quad \ldots \quad z_{n_{mx}} \right] , \qquad (17)$$

and $w_{sb}$ is a search-back window length that is set based on the statistics of the channel. Note that $z_n$ may be any of $z_n^{(ds)}$, $z_n^{(tr)}$, $z_n^{(mt)}$, or $z_n^{(th)}$.

Consider a simple example to illustrate the performance of this searchback algorithm, where a 2-tap channel is analyzed using a single-pulse and single-symbol, and mean absolute error (MAE) of the TOA estimate is compared using simulations and theory. The tap weights are selected as $(0.6, 0.8)$, with a 4ns separation in between, and it is assumed that the center of the blocks are perfectly synchronized to the peak of the received pulses. Assuming that the receiver is already locked to the second block, a searchback is performed to find the last threshold-exceeding sample using $P_{fa} = 0.05$. Theoretically speaking, with the restrictions assumed (since the TOA estimates are assumed to be at the centers of the blocks, and the TOA is restricted to be at block edges due to perfect synchronization), accurately choosing the leading edge block or the previous block yields an error of $0.5t_s = 2$ns, while every neighboring block adds another $t_s = 4$ns error. The theoretical MAE for this simple scenario can be easily derived as in Appendix, and the results in Fig. 5 show that MAE converges to 2ns after 16dB (reaching a 90% confidence of 3ns at 14dB, which is not shown).

However, the received multipath components in typical UWB channels usually arrive at the receiver in multiple clusters, i.e., groups of MPCs that are separated by noise-only samples. In Fig. 6a, the probability density function (PDF) of the number of clusters prior to the peak sample is presented for CM1, and Fig. 6b presents the PDF of the delays between any two clusters *if* there is at least one cluster prior to the peak energy sample. Since the statistics show that there may be delays as large as 20ns between the clusters, the algorithm discussed above may lock to a sample that arrives later than the leading edge.

On the other hand, by allowing a number of consecutive

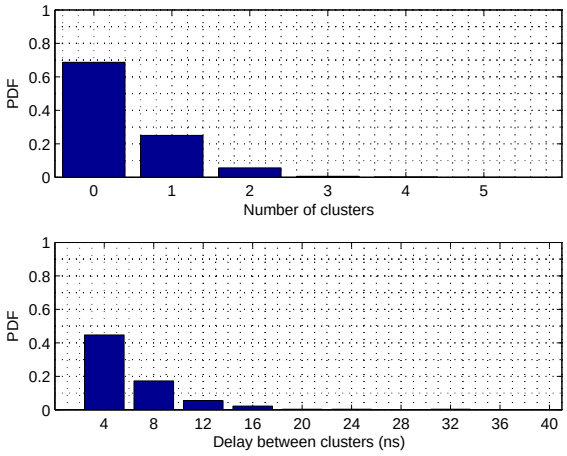


Fig. 6. a) PDF of the number of clusters prior to the peak energy sample, b) The PDF of delays between cluster pairs *if* there is at least one cluster prior to the peak ($T_p = t_s = 4$ns).

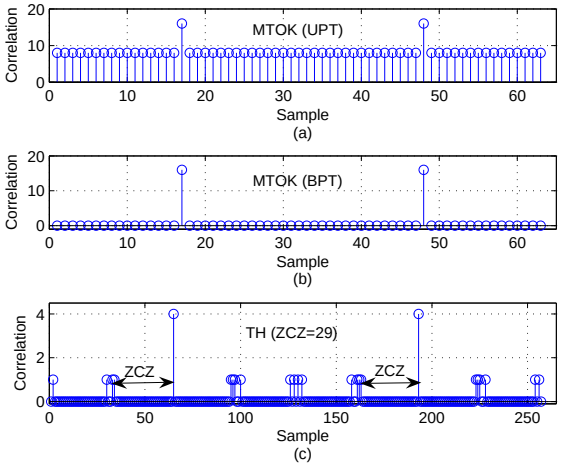


Fig. 7. Periodic code correlations for MTOK-IR and TH-IR (2 periods): a) Periodic MTOK correlation using a uni-polar template (UPT), b) Periodic MTOK correlation using a bi-polar template (BPT), c) Periodic TH-IR autocorrelation.

occurrences of noise samples while continuing the backward search, the clustering problem may be handled. The false alarm probability when $K$ multiple consecutive noise samples are considered can be calculated from

$$P_{fa} = 1 - \left[1 - Q\left(\frac{\xi - \mu_{ed}}{\sigma_{ed}}\right)\right]^K , \qquad (18)$$

which leads to a threshold given by

$$\xi = \sigma_{ed} Q^{-1}\left(1 - (1 - P_{fa})^{\frac{1}{K}}\right) + \mu_{ed} . \qquad (19)$$

Note that the best choice of the threshold is a function of $K$, which is the key idea of this paper. The leading edge estimation is then modified as follows

$$\hat{n} = \text{First}\left\{ n' \middle| \tilde{z}_{n'} > \xi \text{ and } \max\left\{\tilde{z}_{n'-1}, \tilde{z}_{n'-2}, ..., \tilde{z}_{\max(n'-K,1)}\right\} < \xi \right\} + n_{mx} - w_{sb} . \qquad (20)$$

### *A. Trade-off's Between Different Signaling Waveforms for TOA Estimation*

Since the leading edge detection problem discussed above requires searching back the paths prior to the peak, it is susceptible to any kind of interference within the searchback window. Even in the interference-free case, the transmitted sequences should have long enough zero correlation zone (ZCZ) prior to the main lobe of the *periodic* autocorrelation function (ACF); otherwise, the multipath interference from the autocorrelation sidelobes may leak into the searchback window, which may yield erroneous estimates.

The MTOK sequences of length 31 proposed in [6] have optimal correlation characteristics when they are processed with BPT at the receiver. However, this comes in the expense of (almost) doubled noise variance (e.g., compared to a TH case), since the correlation template is of length (almost) twice the number of pulses transmitted (i.e. 16).

The TH sequences, on the other hand, have to be designed appropriately to have a ZCZ. Considering that the MED of the channel can be larger than 100ns for CM1, ideally, the ZCZ has to be larger than $100 + w_{sb}t_s$. While the length of ZCZ increases with the frame duration $T_f$, PAPR requirements enforce that the pulse-to-pulse duration is sufficiently small. In this paper, we restricted the frame duration $T_f^{(th)}$ to 128ns, which yields a code cardinality $N_h = 32$ for $T_c = T_p = 4$ns. Brute-force search of ZCZ codes for $N_s = 4$ yields sequences[1] with ZCZ at most 29 (i.e., 120ns) with a peak to side-lobe ratio (PSLR) of 4. However, the pulse to pulse duration of the sequences may not be *random enough* for smoothing the spectral lines due to ZCZ restriction, and spectral characteristics may have to be adjusted further using the polarity coding. In Fig. 7, the periodic correlations of MTOK and TH sequences are presented over two sequence periods[2].

Compared to MTOK-IR and TH-IR, DS-IR is less susceptible to clustering effects in the searchback step, since the pulses are (almost) consecutively transmitted. As employing the training symbol sequences (with PPM) for piconet separation in DS-IR can be interpreted as a 2-level time-hopping, the ZCZ becomes on the order of $T_{ppm}$, which allows a large window for searchback. The drawback of DS-IR is that it does not exploit the processing gain available, and may perform worse if $N_{sym}$ is not sufficiently large. On the other hand, TR-IR falls in between TH-IR and DS-IR due to the transmitted pulse pairs; it is less affected from clustering problem, and has a larger ZCZ compared to TH-IR, though exploiting only half the processing gain of that of TH-IR.

## IV. Simulation Results

Simulations are performed to compare the TOA estimation errors for different scenarios. In all simulations, $t_s = T_p =$

[1]The search yields 928 sequences, and may further be pruned to leave the ones with good cross-correlation and/or spectral characteristics.

[2]Used MTOK code is $d^{(mt)} = [1\ -1\ -1\ 0\ 0\ 0\ 1\ -1\ 0\ 1\ 1\ 1\ 0\ 1\ 0\ -1\ 0\ 0\ 0\ 0\ 1\ 0\ 0\ -1\ 0\ -1\ 1\ 0\ 0\ -1\ -1]$. Used TH code is $c^{(th)} = [0\ 3\ 3\ 2]$ with $N_h = 32$ and a ZCZ of 29.

TABLE I

COMPARISON OF PARAMETERS AND NOISE STATISTICS FOR DIFFERENT OPTIONS ($M = 4$, $E_s^{(mt)} = 4E_s$).

| | **DS-IR** | **TR-IR** | **MTOK-IR** | **TH-IR** |
|---|---|---|---|---|
| $(N_s, T_{sym}, N_{sym})$ | (4,512ns,8000) | (4,512ns,8000) | (16,1984ns,2000) | (4,512ns,8000) |
| $(T_c, T_f, T_{ppm}, D)$ | (6ns,–,256ns,–) | (4ns,256ns,–,16ns) | (64ns,–,–,–) | (4ns,128ns,–,–) |
| $\mu_{ed}$ | $M\sigma_n^2 = 4$ | $2M\sigma_n^2 = 8$ | $16M\sigma_n^2 - 15M\sigma_n^2 = 4$ | $4M\sigma_n^2 = 16$ |
| $\sigma_{ed}^2$ | $\frac{2M\sigma_n^2}{N_{sym}} = 0.001$ | $2 \times \frac{2M\sigma_n^2}{N_{sym}} = 0.002$ | $31 \times \frac{2M\sigma_n^2}{N_{sym}/4} = 0.1240$ | $4 \times \frac{2M\sigma_n^2}{N_{sym}} = 0.004$ |
| $(w_{sb},\ K)$ | (60ns,2) | (60ns,3) | (60ns,3) | (40ns,3) |
| $\xi, (P_{fa} = 0.0001)$ | 4.1205 | 8.1798 | 5.4004 | 16.2575 |
| $\xi, (P_{fa} = 0.001)$ | 4.1041 | 8.1522 | 5.1983 | 16.2152 |
| $\xi, (P_{fa} = 0.01)$ | 4.0814 | 8.1213 | 4.9550 | 16.1715 |
| $\xi, (P_{fa} = 0.05)$ | 4.0618 | 8.0949 | 4.7470 | 16.1342 |

4ns, and signal bandwidth $B = 500$MHz, yielding a degree of freedom $M = 2Bt_s = 4$. The noise variance $\sigma^2 = N_0/2$ is set to 1, and the symbol energy $E_s$ is scaled to satisfy a certain $E_s/N_0$. The received signal is averaged over a 4ms preamble to suppress noise effects; note that despite the non-coherent averaging, large number of symbols used yields a very large *overall* $E_s/N_0$. The delay $\epsilon$ is taken to be uniformly distributed in $(0, 256)$ns, and the results are averaged over 1000 channel realizations. All the simulations are done using the IEEE 802.15.4a channel models [5], which are the most comprehensive standardized UWB channel models currently available. As unified and fair framework as possible is targeted while analyzing all the schemes, and parameters are adjusted accordingly as illustrated in Table I and Fig. 2.

Simulation results corresponding to CM1 for $P_{fa} \in \{0.0001, 0.001, 0.01, 0.05\}$ are presented in Figs. 8-11. Both the confidence level of obtaining 3ns timing error, and the MAE of the timing error are given. While TH-IR has better energy collection at low $E_s/N_0$, it is seen that the ZCZ is not large enough, and the interference from the sidelobes becomes a problem as the signal energy increases (since the threshold is set based on the noise level only). The sidelobe problem in TH-IR may be alleviated to an extent by designing and employing long-codes, which have similar ZCZ characteristics, and larger PSLRs. On the other hand, DS-IR, MTOK-IR, and TR-IR achieve 90% accuracy as the $E_s/N_0$ increases. Note that the MAE floor is better than that of Fig. 5, and converges to smaller than $2ns$ in all $P_{fa}$'s. This stems from the fact that in Fig. 5, the TOA was restricted to discrete values at the edges of the blocks, and minimum error that can be obtained by choosing the center of the block is 2ns. On the other hand, CM1 simulations assume that the TOA takes continuous values, and simple analysis shows that selecting the center of the block yields an average error on the order of quarter the block size.

## V. CONCLUSION

In this paper, four different signal waveforms are compared for non-coherent TOA estimation. A novel thresholding technique based on noise statistics is presented, which yields accurate leading edge estimates even at low sampling rates, as long as the signal is averaged over many symbols.

## APPENDIX

Let $z_{le}$ denote the leading block sample, $le$ be the leading block index, and $\nu$ blocks are searched prior to the leading block. Then, the MAE can be formulated as

$$\begin{aligned}\text{MAE} &= P\big(z_{le} < \xi\big) \times 1.5t_s + P\big(z_{le} > \xi\big)P\big(z_{le-1} < \xi\big) \times 0.5t_s \\ &+ P\big(z_{le} > \xi\big)P\big(z_{le-1} > \xi\big)P\big(z_{le-2} < \xi\big) \times 0.5t_s + ... \\ &+ P\big(z_{le} > \xi\big)...P\big(z_{le-\nu+1} > \xi\big)P\big(z_{le-\nu} < \xi\big) \times (\nu - 1.5)t_s\end{aligned} \tag{21}$$

which yields

$$\begin{aligned}\text{MAE} = 1.5t_s \times Q\left(\frac{\mu_{le} - \xi}{\sigma_{le}}\right) + \\ \left[1 - Q\left(\frac{\mu_{le} - \xi}{\sigma_{le}}\right)\right] \times \left[0.5t_s \times \left(1 - Q\left(\frac{\xi - \mu_{ed}}{\sigma_{ed}}\right)\right)\right. \\ + 0.5t_s \times Q\left(\frac{\xi - \mu_{ed}}{\sigma_{ed}}\right) \times \left(1 - Q\left(\frac{\xi - \mu_{ed}}{\sigma_{ed}}\right)\right) + ... + \\ \left.(v - 1.5)t_s \times Q\left(\frac{\xi - \mu_{ed}}{\sigma_{ed}}\right)^{v-1} \times \left(1 - Q\left(\frac{\xi - \mu_{ed}}{\sigma_{ed}}\right)\right)\right],\end{aligned} \tag{22}$$

where $\mu_{le}$ and $\sigma_{le}^2$ are the mean and the variance of the leading energy block, while $\mu_{ed}$, $\sigma_{ed}^2$ are the corresponding parameters for noise-only samples. Note that the expressions correspond to perfect synchronization to pulse peak, and error coefficients for choosing a certain block may be formulated differently for a different set of assumptions.

## REFERENCES


[1] S. Gezici, Z. Sahinoglu, H. Kobayashi, and H. V. Poor, *Ultra Wideband Geolocation.* John Wiley & Sons, Inc., 2005, in Ultrawideband Wireless Communications.

[2] N. He and C. Tepedelenlioglu, "Performance analysis of non-coherent UWB receivers at different synchronization levels," in *Proc. IEEE Int. Conf. Global Comm. (GLOBECOM)*, Montreal, Canada, Nov. 2004, pp. 3517–3521.

[3] A. Rabbachin and I. Oppermann, "Synchronization analysis for UWB systems with a low-complexity energy collection receiver," in *Proc. IEEE Ultrawideband Syst. Technol. (UWBST)*, Kyoto, Japan, May 2004, pp. 288–292.

[4] J. Yu and Y. Yao, "Detection performance of time-hopping ultrawideband LPI waveforms," in *Proc. IEEE Sarnoff Symp.*, Princeton, New Jersey, Apr. 2005.

[5] A. F. Molisch et. al., "IEEE 802.15.4a channel model - final report," 2005, tech. rep. doc: IEEE 802.15-04-0662-02-004a. [Online]. Available: http://www.ieee802.org/15/pub/TG4a.html

[6] F. Chin, "Impulse radio signaling for communication and ranging," April, 2004, doc.: IEEE 802.15-05-0231-00-004a. [Online]. Available: http://802wirelessworld.com

[7] I. Guvenc and Z. Sahinoglu, "Threshold-based TOA estimation for impulse radio UWB systems," IEEE Int. Conf. UWB (ICU), Zurich, Switzerland, Sept. 2005, accepted for publication.

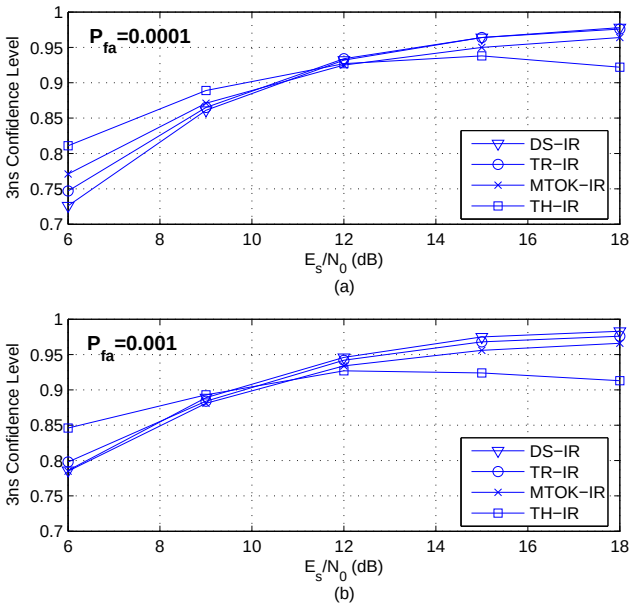


Fig. 8. Confidence level of 3ns for a) $P_{fa} = 0.0001$ and b) $P_{fa} = 0.001$.

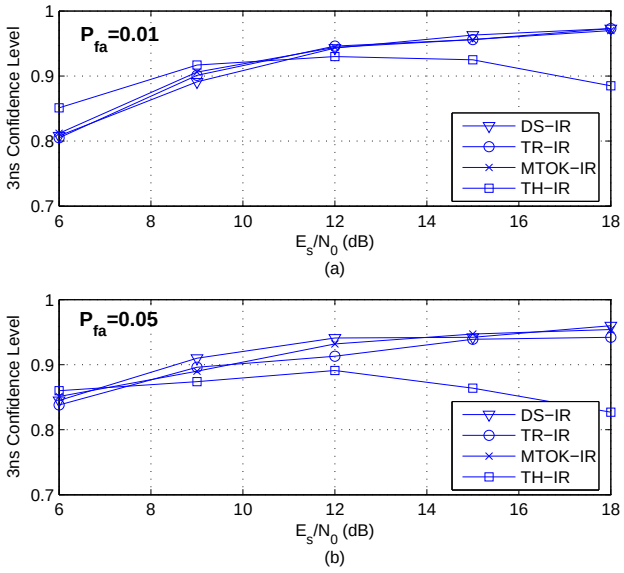


Fig. 9. Confidence level of 3ns for a) $P_{fa} = 0.01$ and b) $P_{fa} = 0.05$.

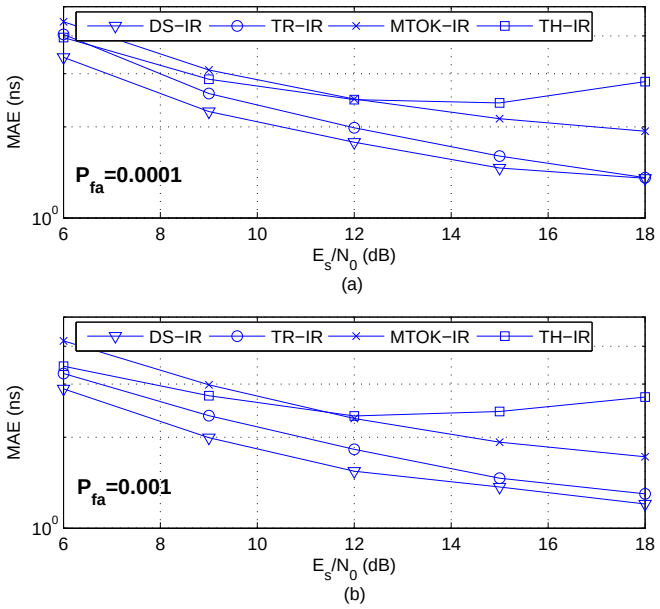


Fig. 10. MAEs for a) $P_{fa} = 0.0001$ and b) $P_{fa} = 0.001$.

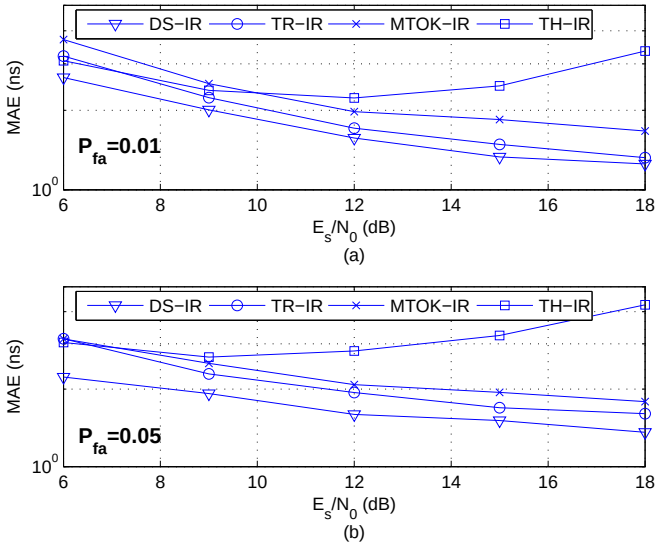


Fig. 11. MAEs for a) $P_{fa} = 0.01$ and b) $P_{fa} = 0.05$.